JACC: BASIC TO TRANSLATIONAL SCIENCE VOL. 8, NO. 3, 2023

ORIGINAL RESEARCH - PRECLINICAL

Reversal of Right Ventricular Remodeling After Correction of Pulmonary Regurgitation in Tetralogy of Fallot

Bjorn Cools, MD, PhD,[a,b,*] Chandan Kadur Nagaraju, PhD,[b,*] Katrien Vandendriessche, MD,[b] Joeri van Puyvelde, MD,[b,c] Mohamad Youness, PhD,[b] H. Llewelyn Roderick, PhD,[b] Marc Gewillig, MD, PhD,[a,b] Karin Sipido, MD, PhD,[b] Piet Claus, PhD,[b] Filip Rega, MD, PhD[b,c]

VISUAL ABSTRACT

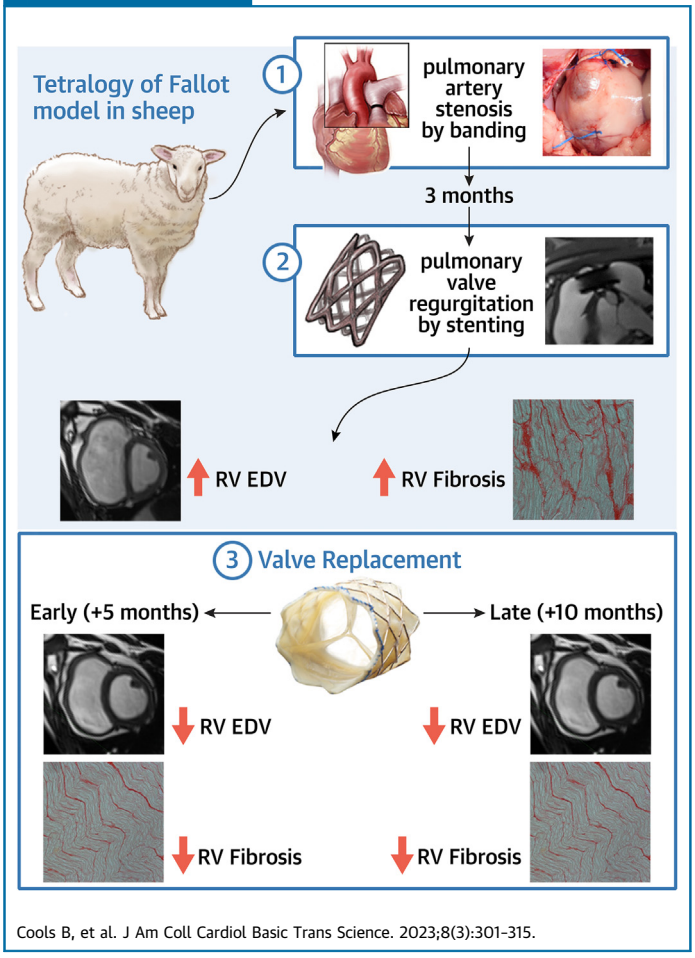

Cools B, et al. J Am Coll Cardiol Basic Trans Science. 2023;8(3):301-315.

HIGHLIGHTS

- A sheep model recapitulating the trajectory of tetralogy of Fallot patients unraveled the in vivo pathophysiology of adverse and reverse remodeling of the RV.
- Severe pulmonary regurgitation with right ventricular volume load led to fibrosis and myocyte hypertrophy, related to altered gene expression directing matrix remodeling.
- Pulmonary valve replacement reduced the fibrotic changes and cardiomyocyte hypertrophy and partially reversed related gene expression and signaling.
- Right ventricular reverse remodeling was not dependent on timing of pulmonary valve replacement in this animal model.

From the [a]Department of Pediatric and Congenital Cardiology, University Hospitals Leuven, Leuven, Belgium; [b]Department of Cardiovascular Sciences, KU Leuven, Leuven, Belgium; and the [c]Department of Cardiac Surgery, University Hospitals Leuven, Leuven, Belgium. *Drs Cools and Nagaraju contributed equally to this work and are joint co-first authors.
Daniel Burkhoff, MD, served as Guest Associate Editor for this paper. Michael Bristow, MD, PhD, as Guest Editor-in-Chief for this paper.

ISSN 2452-302X https://doi.org/10.1016/j.jacbts.2022.09.008

ABBREVIATIONS AND ACRONYMS

BSA = body surface area

CMR = cardiac magnetic resonance imaging

ECM = extracellular matrix

PFA = paraformaldehyde

PICP = C-terminal propeptide of procollagen type I

PR = pulmonary regurgitation

PTFE = polytetrafluoroethylene

PV = pulmonary valve

PVR = pulmonary valve replacement

rTOF = repaired tetralogy of Fallot

RV = right ventricle

RVEDVi = right ventricular end-diastolic volume indexed for body surface area

RVESVi = right ventricular end-systolic volume indexed for body surface area

RVOT = right ventricular outflow tract

SCD = sudden cardiac death

SMA = smooth muscle actin

TOF = tetralogy of Fallot

TR = tricuspid regurgitation

WGA = wheat germ agglutinin

SUMMARY

In the sheep model with pathophysiologic changes similar to patients with repaired TOF, severe PR leads to fibrotic changes in the RV. Pulmonary valve replacement reverses these fibrotic changes. Early valve replacement led to a quick RV recovery, and in time there was no difference in outcome between early and late valve replacement. These data support the benefit of valve replacement for RV function and suggest that there is a margin in the timing of the surgery. The fibrotic changes correlated well with the circulating biomarker PICP, which can have an added value in the clinical follow-up of patients with repaired TOF. (J Am Coll Cardiol Basic Trans Science 2023;8:301–315)

Patients with surgically repaired tetralogy of Fallot (rTOF) often develop severe pulmonary regurgitation (PR) and chronic volume overload of the right ventricle (RV), leading to RV dilation and hypertrophy. The major long-term risks are malignant arrhythmias leading to sudden cardiac death (SCD) and ventricular failure.[1-3] A significant number of patients with rTOF require pulmonary valve replacement (PVR) during their lifetime. Recommendations for PVR in patients with rTOF have been established by the European Society of Cardiology and American Heart Association/American College of Cardiology.[4,5] Surgical conduits and percutaneous valves have a limited longevity, increasing the risk of reintervention.[6-11] The optimal timing of PVR remains a difficult balance between avoiding irreversible RV dysfunction and the need for reintervention.[12-17] The optimal chance for RV reverse remodeling is observed if PVR is performed before the RV dimensions exceed right ventricular end-diastolic volume indexed for body surface area (RVEDVi) >158 mL/m^2 and right ventricular end-systolic volume indexed for body surface area (RVESVi) >82 mL/m^2.[18] PVR has not been proven to alter the risk for ventricular tachycardia or failure, despite RV reverse remodeling.[14,15,17,19-22]

In-depth knowledge of RV remodeling under volume overload is limited. Increased wall stress by pressure overload leads to reactive hypertrophy of cardiomyocytes and fibroblast proliferation.[23] Activated fibroblasts (myofibroblasts) secrete extracellular matrix (ECM) proteins and collagen.[24] The increased collagen deposition is associated with a disproportionate increase in the secretion of collagen I vs collagen III, leading to a change in their relative abundance in the ECM, which may be partially responsible for the increase in RV stiffness following pressure overload.[23] Compared with these data on RV pressure overload, data on RV volume overload are more scarce.[25]

To gain more insight in rTOF RV remodeling and the impact of PVR at different time points, we created an animal model recapitulating a period of RV pressure overload followed by RV volume overload during PR. Subsequently, the PR was corrected by PVR at 2 different time intervals. The first objective was to study the impact of timing of PVR on the RV reverse remodeling process in vivo through repeated imaging. The second objective was to study RV reverse remodeling in response to PVR at the tissue level, examining fibrosis and cardiac myocyte hypertrophy and related gene expression.

METHODS

ANIMAL CARE. The study was conducted in the animal facility of the laboratory of Experimental Cardiac Surgery at KU Leuven (license number LA 1210253) and approved by the Ethical Review Board (project number 024/2014). All in vivo interventions and measurements were performed under general anesthesia: intravenous injection (IV) of 22 mg/kg ketamine (100 mg/mL Nimatek, Dechra) and inhaled veterinary isoflurane (1,000 mg/g Iso-Vet, Dechra) at 5% for induction and 2.5% for maintenance. Analgesia was with 0.03 mg/kg IV buprenorphine (0.3 mg/mL Vetergesic, Ceva) and 0.2 mg/kg IV meloxicam

The authors attest they are in compliance with human studies committees and animal welfare regulations of the authors' institutions and Food and Drug Administration guidelines, including patient consent where appropriate. For more information, visit the Author Center.

Manuscript received February 11, 2022; revised manuscript received September 9, 2022, accepted September 12, 2022.

(20 mg/mL Metacam, Boehringer Ingelheim). For infection prophylaxis, animals received 40,000 IU/kg IV penicillin (Kela Pharma) and 6.6 mg/kg IV gentamycin (Genta-Kel, Kela Pharma). During the endovascular procedures, 100 IU/kg IV heparin was administered every hour. Twenty-four hours before an endovascular procedure, 5 mg/kg IV amiodarone and at the start of the procedure 1 mg/kg IV lidocaine was administered. After PVR (n = 16), animals received 100 mg acetylsalicylic acid orally once daily.

STUDY GROUPS. A total of 38 animals entered the study protocol. Nine animals were excluded from the analysis for the following reasons: ventricular fibrillation (n = 4), stent embolization (n = 2), endocarditis (n = 1), rupture of the PA on balloon dilation (n = 1), and stent dislocation (n = 1). Eight animals were killed at the age of 7.5 ± 0.5 months and constituted the PS group, but they were not included in the analysis because not all histologic analysis could be completed in the group. All study data therefore refer to 21 animals. Eight additional healthy animals were included as control group for that time point. Interventions were initiated in lambs once it became possible for the animal to recover from the surgery after the lactation period (age 4.5 ± 0.5 months).

Figure 1 illustrates the timeline of interventions in the different study groups. In all animals, pulmonary stenosis (PS) was mimicked through pulmonary banding at the age of 4.5 ± 0.5 months. At 7.5 ± 0.5 months the PS was relieved by placing a bare-metal stent across the pulmonary valve to induce PR. After 5 months we killed 6 animals to assess the subsequent effect of remodeling of PS and PR (PR group). In 8 animals, a Melody valve was implanted at 12.5 ± 0.5 months to correct the PR (early PVR group). These animals were followed for another five months before being killed at 17.5 ± 0.5 months The remaining 8 animals received a Melody valve at the age of 17.5 ± 0.5 months (late PVR group). They also were followed for 5 months and then killed at the age of 22.5 ± 0.5 months

Healthy animals (n = 8) who did not have any intervention were killed at the age of 12.5 ± 0.5 months, matching the age of the PR group at the time of death or early valve implantation.

All animals of the early and late PVR study groups completed the series. In the PR group, 1 animal was excluded for further analysis owing to stent dislocation in the weeks after the procedure. One animal from the early PVR group was not included in the tissue analysis because the sampling and analysis were incomplete.

INTERVENTIONAL PROCEDURES. Creation of the supravalvular pulmonary stenosis. A left-side thoracotomy in the fourth intercostal space was performed at mean age 4.5 ± 0.5 months (lamb stage). The supravalvular pulmonary artery was banded at the level of the sinotubular junction of the pulmonary trunk with the use of a polytetrafluoroethylene (PTFE) strip sutured to the vessel wall to avoid displacement and migration. A radio-opaque marker was sutured onto the PA banding and subvalvular level (Figure 1A).

Relief of the pulmonary stenosis and creating pulmonary regurgitation. Invasive hemodynamics were obtained, subsequently the PS was dilated, and PR was created percutaneously. Left jugular venous access was provided and the PS was fully dilated with the use of a 22-mm high-pressure balloon (Atlas Gold, Bard) with a pressure insufflator. A bare metal stent was delivered on a 22-mm BIB-balloon (Numed) into the right ventricular outflow tract (RVOT) across the pulmonary valve (PV). Stent types used were 45-mm CP-stent (Numed; n = 16) and 43-mm AndraStent XXL (Andramed; n = 8) (Figure 1B).

Pulmonary valve replacement. A Melody valve (Medtronic) was implanted at the age of 12.5 ± 0.5 months in the early PVR group (n = 8) and at the age of 17.5 ± 0.5 months in the late PVR group (n = 8).

Partial (2.5 L/min) extracorporeal membrane oxygenation support was used to maintain circulation while placing the valve through jugular access. The Melody valve was delivered on a 22-mm Melody TPV Ensemble II (Figure 1C).

IN VIVO STRUCTURAL AND FUNCTIONAL ANALYSIS OF RV REMODELING AND REVERSE REMODELING IN RESPONSE TO PVR. All animals underwent cardiac magnetic resonance imaging (CMR) (3-T Magnetom Prisma, Siemens Healthineers) at scheduled intervals: 1) before the relief of the PS and creation of the pulmonary valve regurgitation (1-2 weeks); 2) after creation of the PR (1-2 weeks); 3) before valve replacement (1-2 weeks); 4) after valve placement (1-2 weeks); and 5) at death. The control group had 1 CMR study. All scans were performed in right decubitus position, during suspended respiration and electrocardiographic gating. Morphologic and functional parameters were obtained from steady-state free-precession cine loops in short-axis acquisition covering both left and right ventricles, including PA banding diameter and stent or valve position.

Left ventricular (LV) and RV volumes, mass, stroke volume, and ejection fraction were obtained by means of slice-by-slice manual contouring of the endocardial and epicardial border in systolic and

FIGURE 1 Timeline and Interventional Schedule

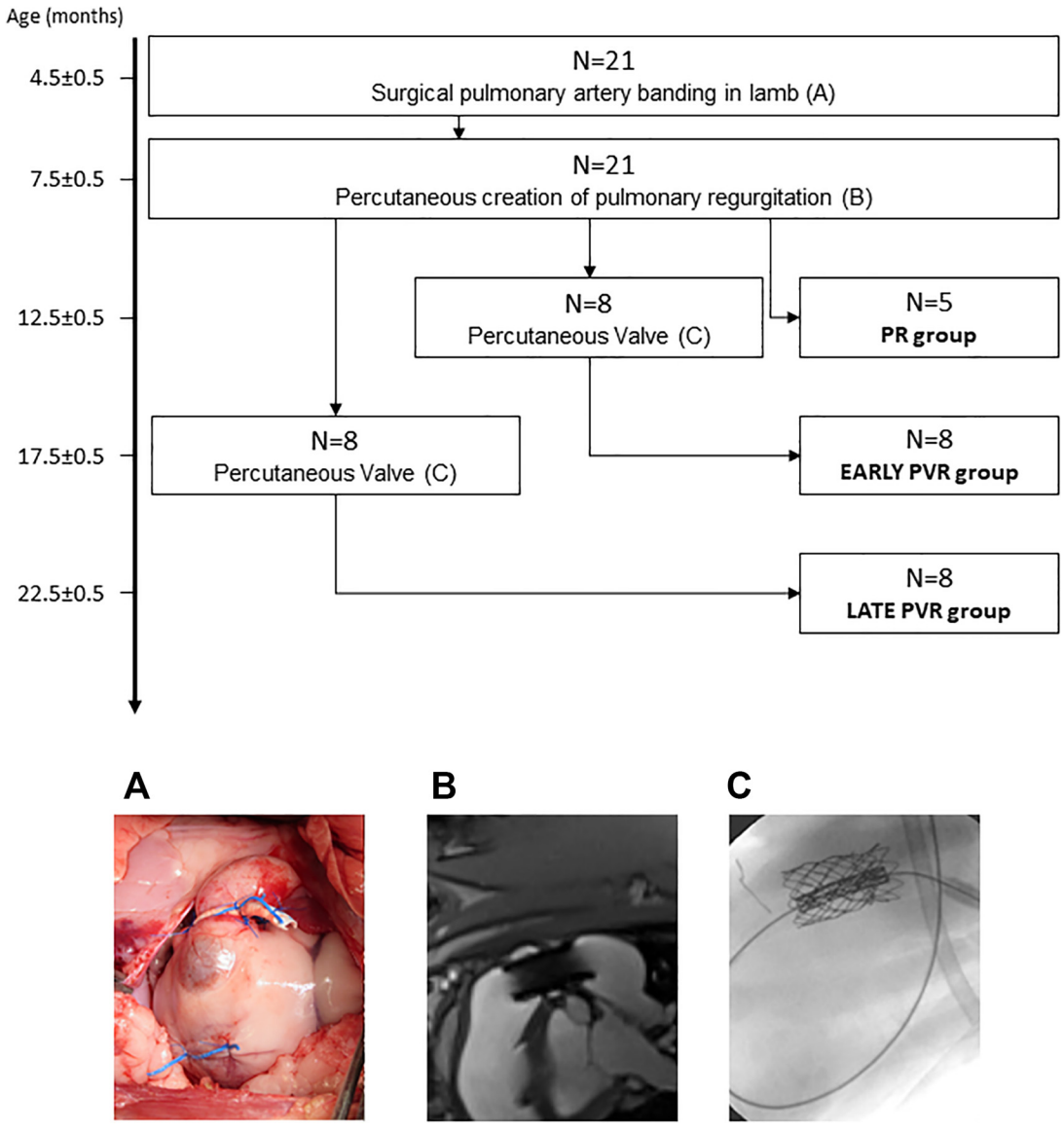

(A) Circular polytetrafluoroethylene (PTFE) strip at the sinotubular junction tightened and sutured with Prolene 5/0 and fixed with 2 stitches (Prolene 5/0) at the wall of the pulmonary trunk. Radio-opaque marker fixed at the PTFE strip and at the subvalvular level to facilitate the stent implantation later. **(B)** Cardiac magnetic resonance image of bare-metal stent across the pulmonary valve. **(C)** Angiographic image of Melody valve implantation in stent with extracorporeal membrane oxygenation cannula. PR = pulmonary regurgitation; PVR = pulmonary valve replacement.

diastolic phases. The papillary muscles were excluded from the tracing. In the RV mass calculation, only the RV free wall was used; the septum was excluded. Ventricular mass was calculated from the ventricular wall volume using the density of myocardium of 1.05 g/mL.[26] Pulmonary and tricuspid valve flows and regurgitation fraction were calculated on phase contrast images. PR was calculated by quantifying the reversal of diastolic flow on the phase-contrast images acquired perpendicular to the

PA and distal from the PV. Data were indexed for body surface area (BSA) with use of the Mitchell formula, $0.09 \times W^{0.67}$, where appropriate.[27] Data were analyzed with the use of Costiul software (RightVol, KU Leuven), which has been validated and described previously.[28]

EX VIVO TISSUE ANALYSIS OF RV REVERSE REMODELING IN RESPONSE TO PVR. At the end of the study protocol, animals were killed under general anesthesia by IV injection of 0.7 mL/kg pentobarbital (Dolethal, Vetoquinol). The heart was removed, and samples taken from the RV and LV. The tissue samples were fixed in 4% paraformaldehyde (PFA) and Tissue-Tek OCT (Sakura Finetek) and snap frozen at −80 °C.

Fibrosis quantification. Samples were processed in histokinette and embedded in paraffin. Tissue sections of 8 μm thickness were deparaffinized and stained with the use of a Sirius red kit (Polysciences). The sections were imaged with the use of a Zeiss Axioplan microscope with a ×10/0.3-NA Ph1 objective. Based on the birefringence properties of collagen using polarized light, the collagen subtypes were quantified: type I thick fibers (red-yellow) and type III thin fibers (green).[29] Fibrosis and collagen subtypes were quantified in the collected images in a blinded manner with the use of Axiovision software, after which data was unblinded.

C-terminal propeptide of procollagen type I measurement. Blood samples were taken with the use of a BD Vacutainer K2 EDTA tube immediately before interventions (before banding of the PA, before PR was created, before PVR) and at death. The serum C-terminal propeptide of procollagen type I (PICP) level was quantified with the use of a competitive enzyme-linked immunosorbent assay kit, according to the manufacturer's instructions (ABIN1057544, Antibodies-Online).

Immunofluorescence staining: myofibroblasts. The presence of alpha-smooth muscle actin (αSMA)-positive cells, a marker for myofibroblasts, was quantified as previously described.[30] Eight-micrometer-thick cryosections were fixed in 2% PFA for 15 minutes and permeabilized with 0.2% Triton-X100 for 20 minutes at room temperature. Sections were blocked with 2% bovine serum albumin for 30 minutes and subsequently incubated overnight at 4 °C with αSMA antibody (1:250 dilution; A2547, Sigma-Aldrich). Next, the sections were washed and incubated with a goat antimouse Alexa Fluor 488 secondary antibody (1:500 dilution; A28175, ThermoFisher Scientific) and further labeled with Alexa Fluor 647 conjugated wheat germ agglutinin (WGA) and mounted with the use of Prolong Gold antifade with 6-diamino-2-phenylindole (ThermoFisher Scientific). Imaging and quantification were performed as previously described.[30]

Gene expression analysis. Total RNA was isolated with the use of the RNeasy kit (1062832, Qiagen), according tothe manufacturer's instructions. cDNA synthesis was carried out using the Superscript Vilo kit on equal quantities of RNA per sample (11754050, Thermofisher Scientific). The obtained cDNA was diluted 1:20 in nuclease-free water before quantitative polymerase chain reaction, which was set up in 384 well plates and analyzed as previously described.[29] Gene expression was normalized to the mean of 2 reference genes (*YWHAZ*, *RPL19*). The primers were commercially purchased from Integrated DNA Technologies, and the sequences are presented in Supplemental Table 1.

Myocyte hypertrophy. From tissue samples embedded in Tissue-Tek OCT compound, 8-μm-thick sections were prepared. The tissue sections were fixed in 2% PFA and incubated with Alexa Fluor 647 Conjugated WGA (ThermoFisher Scientific) to label their outlines for 1 hour. The sections were mounted with Prolong Gold antifade mountant and imaged with a Nikon A1R confocal microscope configured on a Ti2 microscope using a Plan ×40 Oil DIC H/N2 objective. Four random areas in nonfibrotic regions were imaged. Horizontal and vertical lines of 165 μm size were drawn on each image and the number of transected cardiomyocytes was counted; fewer cells transected indicates larger hypertrophic cells.[31]

STATISTICAL ANALYSIS. Statistical analysis was performed using SPSS version 26 (IBM) and tools available in Prism 8 (GraphPad). Normality was assessed by means of the Kolmogorov-Smirnov test. Normality was not violated. Comparisons among different groups were done by means of ANOVA with Tukey's post hoc test for multiple pairwise comparisons. Comparison of paired data was carried out using a 2-tailed paired Student's *t*-test. Continuous data are expressed as mean ± SD or SEM. Simple linear regression was used for correlation analysis. Statistical significance was accepted with a P value <0.05.

RESULTS

IN VIVO STRUCTURAL AND FUNCTIONAL RV REMODELING AND REVERSE REMODELING IN RESPONSE TO PVR.

Pulmonary artery banding and induction of regurgitation. Three months after pulmonary artery banding, mild stenosis was present in all animals with a measured invasive peak-to-peak gradient of 11.6 ± 3.6 mm Hg.

FIGURE 2 **In Vivo Structural and Functional Right Ventricular Remodeling and Reverse Remodeling**

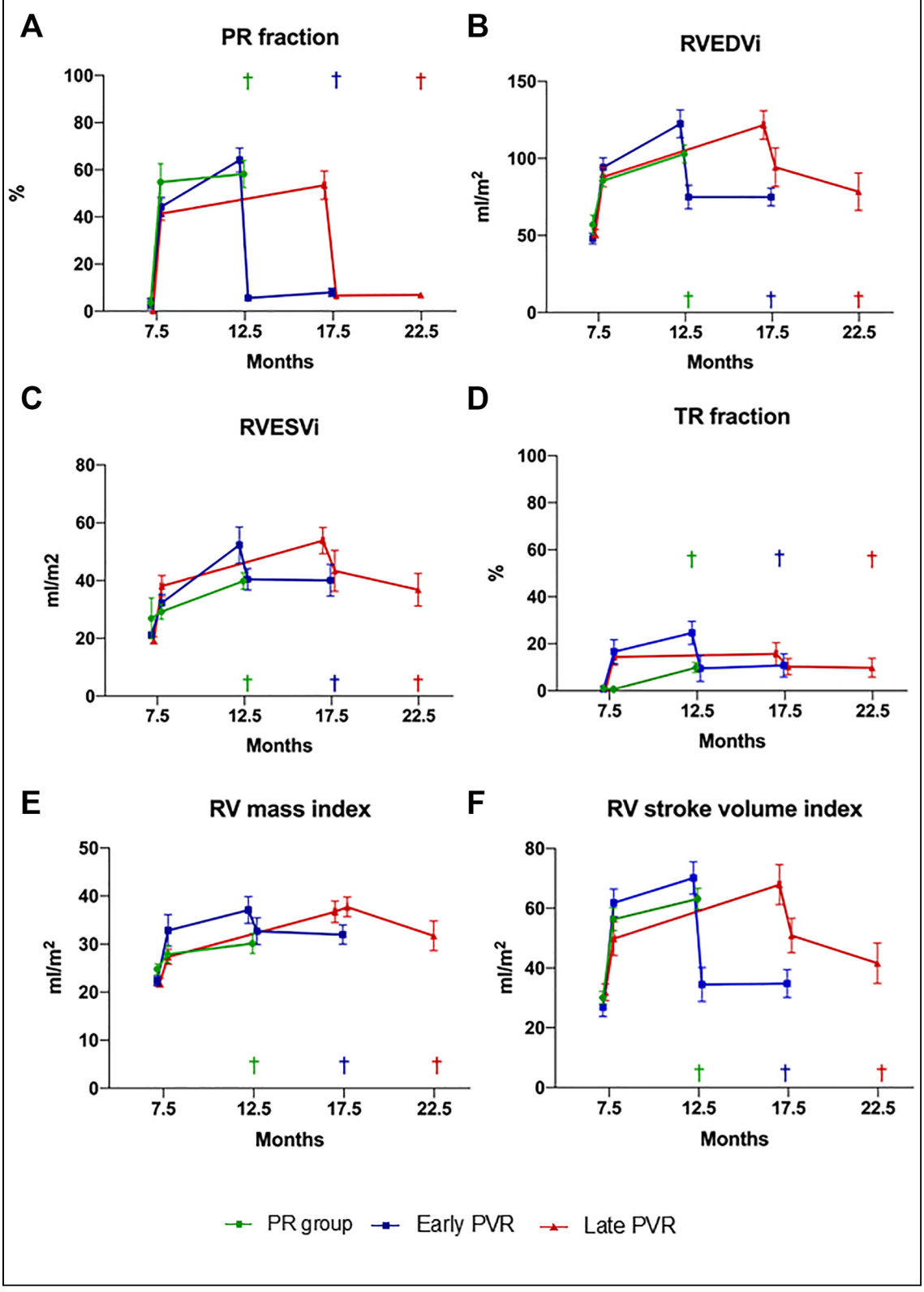

Continued on the next page

Relieving the pulmonary artery stenosis by balloon dilation resulted in a significant reduction of the RV-to-PA peak-to-peak gradient (3 ± 2 mm Hg) (P = 0.001). Implantation of the stent across the pulmonary valve induced severe regurgitation, as shown in Figure 2A. The PV indexed regurgitant volume increased significantly from 0.7 ± 1.1 mL to 23.1 ± 5.1 mL (P = 0.000) after dilation.

RV remodeling in response to pulmonary regurgitation. The pulmonary regurgitation gave rise to a significant increase in the RV dimensions within 10 days of stent placement, with some further increase in the 5-month follow-up. The evolution of the RVEDVi is shown in Figure 2B, presented separately for the PR, early PVR, and late PVR groups. The RVESVi also increased significantly in both groups (P = 0.019 and P = 0.001) with ΔRVESVi 16.5 ± 10.1 in early PVR and 18.8 ± 9.0 in late PVR (Figure 2C, Table 1, Supplemental Table 2). The mass-to-volume ratio decreased significantly after PR in all subgroups, with significantly increased RV mass (Figure 2E). The RV-to-LV diastolic ratio, however, increased significantly owing to the RV dilation (P = 0.002 and P = 0.000) (Supplemental Table 2). Tricuspid regurgitation (TR) was observed within 2 weeks after creation of PR in both study groups with a ΔTR fraction in early PVR of 16.0 ± 14.6 and in late PVR of 13.4 ± 10.1 (Figure 2D).

Pulmonary valve replacement and immediate response. There was no difference between early and late PVR regarding RV mass and RV volume indexes at 5 and 10 months of PR (Figures 2E and 2F). Once PVR was performed, the pulmonary regurgitation fraction and the indexed PV regurgitant volume improved acutely in the early and the late PVR group, as shown in Figure 2A. RVEDVi and RVESVi decreased significantly in both PVR groups (P = 0.000 and P = 0.049) (Figures 2B and 2C). Within 2 weeks after PVR, recovery from dilatation of the RV was observed in the early PVR group (ΔRVEDVi 47.5 ± 17.8 mL/m^2) (Table 1). This effect was less pronounced in late PVR (ΔRVEDVi 27.5 ± 12.5 mL/m^2) (P = 0.021). TR decreased significantly in the early PVR group after PVR (P = 0.026) with a ΔTR fraction of −15.1 ± 15.2 in early PVR compared with −3.4 ± 7.0 in late PVR (Table 1).

RV reverse remodeling after PVR. Both early and late PVR groups were followed for 5 months after valve implantation. At that time point, the changes in RV diastolic and systolic volumes and dimensions were similar for both groups. The RV mass-to-volume ratio had increased significantly in both early and late PVR (P = 0.001 and P = 0.009) (Supplemental Tables 3 and 4). The RV-LV systolic and diastolic ratios remained unchanged in both early and late PVR groups. RV mass decreased significantly after PVR in both groups (P = 0.018 and P = 0.006) (Figure 2E). LV systolic and diastolic dimensions did not change during follow-up (Supplemental Table 4). Animals in early and late PVR were killed at 5 months after PVR.

RV REMODELING AND REVERSE REMODELING IN RESPONSE TO PVR AT THE TISSUE LEVEL. To study structural changes in the RV matrix, we analyzed interstitial fibrosis and collagen cross-linking after chronic PR and examined whether PVR altered fibrosis (Figure 3A). Interstitial fibrosis and the abundance of type I collagen, indicative of cross-linking was increased several-fold in PR compared to control (Figures 3B and 3C). Fibrosis was significantly lower in both early and late PVR 5 months after PVR compared with PR, with no significant difference between early PVR and late PVR (P = 0.81). Optimally, we would have repeatedly sampled myocardial tissue in the same sheep, but this was not possible. As a surrogate, we analyzed circulating blood levels of PICP, a biomarker for the synthesis of collagen type I at each time point (Figure 3D). PICP increased from the moment of PA banding, with highest values detected at chronic PR (P < 0.05). In early and late PVR, the PICP levels decreased after PVR (P = 0.16 and P = 0.014, respectively, 2-tailed paired Student's t-test) but remained elevated compared with control. The PICP levels correlated well with fibrosis, although scatter was substantial (Figure 3E).

Given the major role of activation of fibroblasts and their differentiation into myofibroblasts in cardiac remodeling, we also probed for the presence of myofibroblasts. To this end, we counted the number of interstitial cells that were positive for αSMA (Figure 4A). Compared with the PR group, the number of αSMA-positive cells was significantly lower in both

FIGURE 2 Continued

(A) Pulmonary regurgitation (PR) fraction over time. **(B)** Evolution of right ventricular end-diastolic volume indexed for body surface area (BSA) (RVEDVi) after interventions. **(C)** Evolution of right ventricular end-systolic volume indexed for BSA (RVESVi) after interventions. **(D)** Tricuspid regurgitation (TR) fraction over time. **(E)** RV mass indexed for BSA over time. **(F)** RV stroke volume over time. All: early pulmonary valve replacement (PVR; n = 8), late PVR (n = 8), PR group (n = 5). RV = right ventricular.

TABLE 1 Differences in. Magnetic Resonance Imaging Observations Expressed as Delta (Δ) Between Study Groups

	Δ Before vs After Stent			Δ Before vs After PVR			Δ After PVR vs Death		
	Early (n = 8)	Late (n = 8)	*P* Value	Early (n = 8)	Late (n = 8)	*P* Value	Early (n = 7)	Late (n = 8)	*P* Value
PR fraction, %	41.9 ± 14.1	41.1 ± 7.9	0.88	−38.7 ± 11.7	−34.7 ± 6.1	0.41	2.0 ± 3.9	0.3 ± 2.8	0.22
PV regurgitant volume, mL	23.6 ± 5.1	21.0 ± 5.8	0.35	−30.1 ± 9.9	−21.5 ± 8.2	0.07	0.6 ± 1.0	−0.2 ± 0.6	0.08
TR fraction	16.0 ± 14.6	13.4 ± 10.1	0.67	−15.1 ± 15.2	−3.4 ± 7.0	0.06	0.1 ± 6.1	−0.5 ± 6.1	0.79
RVEDVi, mL/m^2	58.1 ± 23.2	36.7 ± 16.7	0.05	−47.5 ± 17.8	−27.5 ± 12.5	0.021[a]	−3.5 ± 8.4	−15.8 ± 9.6	0.021[a]
RVESVi, mL/m^2	16.5 ± 10.1	18.8 ± 9.0	0.62	−11.8 ± 14.0	−10.4 ± 15.0	0.85	−0.3 ± 9.0	−6.6 ± 6.5	0.19
RV-LV diastolic ratio	1.1 ± 0.5	1.1 ± 0.2	0.64	−1.2 ± 0.5	−0.7 ± 0.2	0.019[a]	0.1 ± 0.3	−0.1 ± 0.4	0.53
RV-LV systolic ratio	0.6 ± 0.4	0.5 ± 0.3	0.53	−0.4 ± 0.6	−0.3 ± 0.4	0.73	0.1 ± 0.3	−0.3 ± 0.6	0.11
RV mass indexed, mL/m^2	16.1 ± 12.0	5.3 ± 5.2	0.032[a]	−4.4 ± 4.0	1.0 ± 5.9	0.05	−1.6 ± 5.5	−6.0 ± 4.4	0.15
RV mass-to-volume ratio	0.0 ± 0.2	−0.1 ± 0.1	0.14	0.1 ± 0.1	0.1 ± 0.1	0.90	−0.1 ± 0.2	0.0 ± 0.1	0.90

Values are mean ± SD. [a]$P < 0.05$.

PR = pulmonary regurgitation; PV = pulmonary valve; TR = tricuspid regurgitation; RVEDVi = right ventricular end–diastolic volume indexed for body surface area; RVESVi = right ventricular end–systolic volume indexed for body surface area; LV = left ventricle; PVR = pulmonary valve replacement.

early PVR (P <0.001) and late PVR (P <0.001). There was no difference between early and late PVR (P = 0.91) (Figure 4B). The density of myofibroblasts correlated well with the degree of collagen deposition (Figure 4C).

To gain insight into the mechanisms of fibrosis and underlying signaling, we assessed changes in expression of genes related to matrix remodeling. In PR, the expression of all genes analyzed was increased several-fold over control. Collagen type I was significantly reduced after PVR, whereas lysyl oxidase, promoting collagen cross-linking, did not reach significance (Figures 4D and 4E). The expression of periostin, which can directly interact with collagen type I, also was reduced after late PVR in contrast to early PVR (Figure 4F). The gene expression of matrix metalloproteinase 2 was significantly reduced after PVR (Figure 4G).

We further assessed the impact of the RV load during PR and subsequent PVR on cardiomyocyte hypertrophy. Cardiomyocyte size was analyzed in tissue sections stained with WGA (Figure 5A) by measuring the number of transected cardiomyocytes in a line of fixed length, a smaller number indicating a larger cell diameter. Hypertrophy was most pronounced in the PR group, and significantly different between the early and late PVR groups (Figure 5B). In line with cardiomyocyte hypertrophy, gene expression of the hypertrophy markers natriuretic peptide (NPP) A and B was most elevated in the PR group, and the reduction after PVR was statistically significant only for NPPA (Figure 5C). In Figure 5B we present the data for wall thickness of the free RV wall as measure of myocardial hypertrophy and show that this parameter correlated with measurement of cellular hypertrophy.

DISCUSSION

OVINE MODEL TO STUDY SECONDARY PR AND PVR IN rTOF. A sheep model resembling the clinical course of patients with TOF was created to study RV reverse remodeling after PVR as well as the timing of PVR itself.[12,16] Data on RV reverse remodeling after PVR in patients with rTOF exist, but data on reverse remodeling of myocytes and ECM are lacking.[14]

Most animal studies where PS and/or PR is created are performed in pigs.[32-34] A significant advantage of our sheep model is the more modest weight gain, allowing longer follow-up (+36% in sheep vs +127% in pigs over 3 months). This growth difference could explain why the RVOT gradient is higher in the pig models.[34] The downside is a milder PS in sheep.

Compared with other animal models, our approach to create PR was different. We used a bare-metal stent to create PR over external suture plication, leaflet resection, or transannular patch.[34-39] The use of a bare metal stent in the RVOT is known to induce severe pulmonary regurgitation and RV dilation in animal models.[40-42] Later on, the stent enabled a good stable positioning of the Melody valve.

The procedural time points in our model were chosen in relation to the clinical decision moments we experience over the lifetime of a patient with TOF. The age of 12.5 ± 0.5 months for early PVR and 17.5 ± 0.5 months for late PVR was chosen based on the key physiologic milestones and weight gain of the sheep. Wang et al[43] described a quantitative translation of dog-to-human aging, based on a comparison of DNA methylation. Similar more specific ovine data do not exist, but using the logarithmic scale of Wang et al, early PVR corresponds to a human age of 15 to 25 years and late PVR to 30 to 40

FIGURE 3 **Fibrosis in Pulmonary Regurgitation and Reverse Remodeling After Pulmonary Valve Replacement**

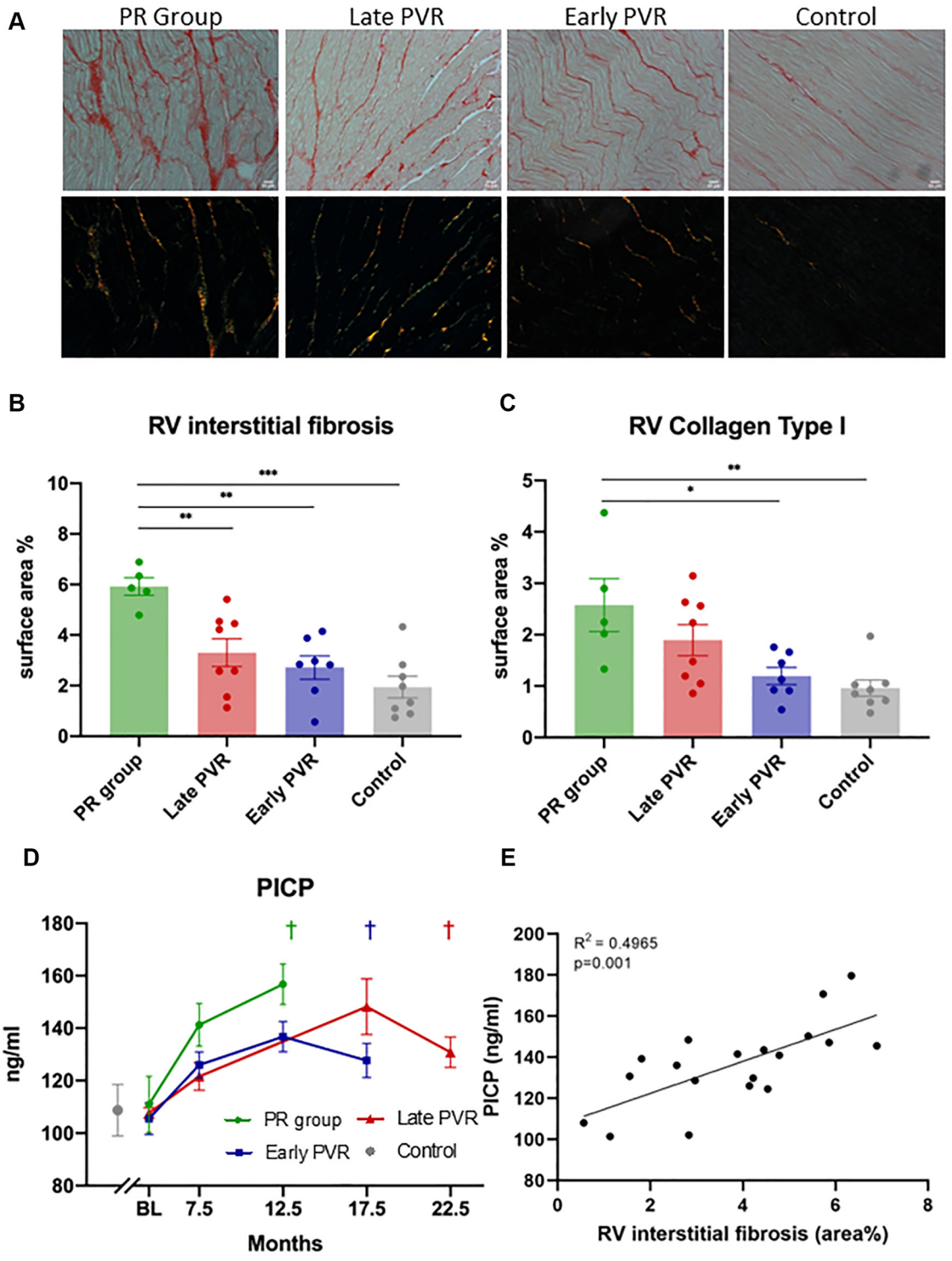

Continued on the next page

years. Although the match may not be perfect, this ovine model allowed us to study the response to PVR across the spectrum of in vivo, cellular, and molecular remodeling.

IN VIVO STRUCTURAL AND FUNCTIONAL RV REMODELING AND REVERSE REMODELING IN RESPONSE TO PVR. The changes consequent to the PS, present at the time of induction of PR, are consistent with earlier findings in pressure overload, ie, an increase in RV mass without dilation.[23,44,45] The subsequent hemodynamic changes due to superimposed volume overload were as expected with substantial RV dilation. In this study, the RV mass-to-volume ratio also decreased during PR similarly as in patients with rTOF.

Within 2 weeks after PVR, we saw a significant reduction of the RV dilation, with slower progression in the subsequent months. This time course is similar to what we observe in patients with TOF, where RV reverse remodeling is seen immediately after PVR and reverse remodeling continues up to 3 years after PVR.[18] The early reduction was more pronounced in the early PVR group, but the eventual reverse remodeling was similar in both groups, although neither volume nor mass returned to values of the control group, as also observed at the tissue level.

The difference of immediate response between early and late PVR groups needs cautious interpretation as factors unrelated to the correction of PR may influence reverse remodeling. The RV dilation during PR can lead to TR in the absence of structural damage to the tricuspid valve. Variability between animals in the presence of TR would influence the remodeling process, as suggested in a post hoc analysis of our data. This hypothesis requires further study, to be pursued in both experimental and clinical settings.

EX VIVO TISSUE ANALYSIS OF RV REVERSE REMODELING IN RESPONSE TO PVR. Reverse remodeling of matrix and cardiomyocytes was documented by tissue samples obtained at the time of death, with the PR group as reference. These data indicated that there is reduction of fibrosis and reverse matrix remodeling 5 months after PVR, to the same extent in both early and late PVR, except the expression of periostin did not decrease in late PVR, in contrast to early PVR. This might explain the less pronounced reduction of collagen type I in late PVR, because periostin can directly interact with collagen I.[46,47]

Serial sampling of PICP, a biomarker for the synthesis of collagen type I, confirmed the presence of reverse remodeling.[48] Nevertheless, the levels of fibrosis and PICP did not fully return to those of healthy animals of the same age as the PR group. Likewise, cardiomyocyte hypertrophy regressed significantly, but again, not reaching the cell size seen in healthy animals. Gene expression patterns also support some degree of matrix remodeling, but eg, signaling toward collagen cross-linking and matrix degradation was not (yet) significantly downregulated.

The incomplete reversal of remodeling may be due to the relatively early evaluation, but other factors could also contribute. As with the in vivo remodeling, the presence of TR can affect the extent and time course of reverse remodeling. The PICP data also suggest an important remodeling related to the first phase of pressure overload, exacerbated by the volume overload. Little is known about the compound effects of these insults, requiring further research into related signaling pathways.

CLINICAL EVIDENCE FOR REVERSE REMODELING AND FUTURE RESEARCH PERSPECTIVES. In patients with rTOF, an expansion of the extracellular volume (ECV) fraction was observed with the use of T1 mapping, which reflects the ratio of ECM volume to total myocardial volume.[49] This increased ECV was demonstrated in RV volume overload and was negatively related to RV mass-to-volume ratio. The authors[49] speculated that in patients with TOF with RV volume overload, an increased ECV with decreased mass-to-volume ratio correlates with a maladaptive process characterized by diffuse fibrosis and loss of cardiomyocytes. Our findings at the tissue level support the idea that increased ECV and decreased mass-to-volume ratio on CMR correspond to increased fibrosis because of activated fibroblasts and increased cross-linked collagen. However, the experimental

FIGURE 3 Continued

(A) Tissue sections of 8 μm size stained with Sirius Red. Quantification of interstitial fibrosis using polarized light, the collagen subtypes were quantified: type I thick fibers **(red/yellow)** and type III thin fibers **(green)**. Images of **(top row)** Sirius Red staining and **(bottom row)** polarized light. **(B)** Right ventricular (RV) interstitial fibrosis; Sirius Red staining, polarized light: PR (n = 5), late PVR (n = 8), early PVR (n = 7), control (n = 8). **(C)** RV collagen type I: PR (n = 5), late PVR (n = 8), early PVR (n = 7), control (n = 8). **(D)** Evolution over time of C-terminal propeptide of procollagen type I (PICP) level: PR (n = 5), late PVR (n = 8), early PVR (n = 7), control (n = 8). †means sacrifice. **(E)** Correlation of RV fibrosis and PICP. Comparisons among different groups were done by means of ANOVA with Tukey's test. *$P < 0.05$; **$P < 0.01$; ***$P < 0.001$. Abbreviations as in Figure 1.

FIGURE 4 **Inactivation of Myofibroblasts and Gene Expression for Matrix Remodeling in Response to Pulmonary Valve Replacement**

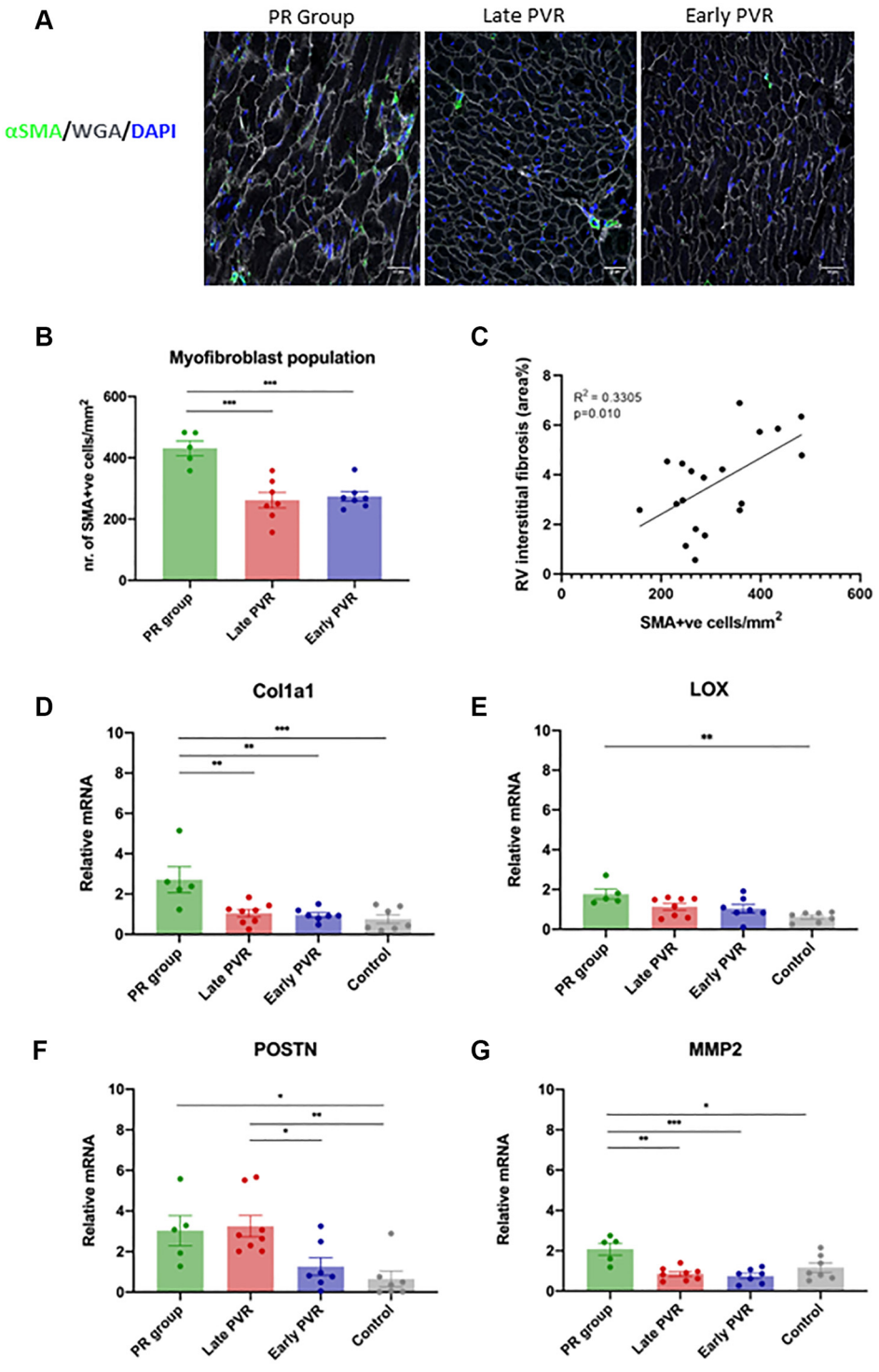

Continued on the next page

data are not in line with cardiomyocyte atrophy but rather show a hypertrophic response of the RV cardiomyocytes. In a recent study, severe fibrosis was documented and correlated with increased RV mass and increased RVESVi in adult rTOF patients undergoing surgical PVR.[50]

Fibrotic changes due to RV volume overload have not been studied to the same extent as pressure overload, but several studies using CMR are consistent with RV fibrosis in patients with rTOF. Kozak et al found in 18 children with rTOF shorter postcontrast T1 values of the RV anterior wall compared with healthy children, suggesting a higher degree of fibrosis.[51] CMR signs of fibrosis correlate with different factors, such as the presence of pressure overload, late repair, and increased patient age, and signs of fibrosis can be present in children early after repair.[52] In adults with rTOF, higher PICP levels correlated with larger RV volumes and higher RV LGE on CMR.[48] In patients with rTOF, myocardial fibrosis is a key element of the maladaptive response to chronic hemodynamic overload, and its onset precedes ventricular dysfunction.[49]

The presented data show that severe PR leads to fibrotic changes in the RV with increased signaling, which has an important added value to the clinical findings of CMR studies in patients with rTOF. More importantly, PVR reverses these fibrotic changes with decreased signaling, which supports the benefit of valve replacement to preserve the RV. Although the timing of PVR in this model did not affect the eventual RV reverse remodeling, early PVR led to more rapid RV reverse remodeling process suggesting that there is a margin in the timing of valve replacement. The fibrotic changes correlated well with the circulating biomarker PICP. This biomarker can have an added value in the clinical follow-up of patients with rTOF and might become helpful for decision making.

The present experimental work suggests that combining functional and structural imaging with circulating biomarkers may provide stronger guidance in the clinical setting and will be the subject of future studies.

STUDY LIMITATIONS. Our animal model mimics features that we see in patients with TOF. We started, however, with structurally normal hearts without overriding of the aorta and a ventricular septum defect. A TOF-phenotype sheep does not exist. A surgical stenosis was created as early as possible in the life of the lamb, which was after lactation, around 18 to 20 weeks. In this way the animal was able to recover from the surgery in absence of its mother. The observed changes on the heart, therefore, do not correspond to the changes seen in a true congenital tetralogy of Fallot. This is an important shortcoming of our model.

The optimal study design to document reverse remodeling would have been to sequentially sample myocardial tissue at different interventional time points and correlate these observations with the CMR findings. However, serial pre-elevation of full thickness myocardial tissue might have led to an increase in myocardial scarring and increased loss of animals, precluding this approach. TR was observed after stent placement in both study groups.

Diffuse fibrosis may have an impact on diastolic function with impaired relaxation and restrictive filling patterns; unfortunately, this could not be evaluated in the animals owing to absence of dedicated software at the animal research facility. Also, CMR imaging of diffuse fibrosis was technically not possible in the first years of the study.

The arrhythmic risk and its relation to fibrosis were not analyzed, and no malignant arrhythmia was observed in these animals apart from a low threshold for developing ventricular fibrillation upon advancing large sheaths into the RVOT.

CONCLUSIONS

This sheep model shows pathophysiologic changes similar to patients with rTOF and the benefit of correction of PR. PR leads to important structural

FIGURE 4 Continued

(A) Immunofluorescent staining of α-smooth muscle actin (SMA) **(green)** and nucleus 6-diamino-2-phenylindole (DAPI) **(blue)**, and wheat germ agglutinin (WGA). **(B)** Density of myofibroblast cells with αSMA staining: pulmonary regurgitation (PR) (n = 5), late PVR (n = 7), early PVR (n = 7). **(C)** Correlation between fibrosis and myofibroblast differentiation. **(D to F)** mRNA expression for matrix remodeling: **(D)** collagen type 1 (Col1a1), **(E)** lysyl oxidase (LOX), **(F)** periostin (POSTN), **(G)** matrix metalloproteinase 2 (MMP2): control (n = 7), PR (n = 5), early PVR (n = 7), late PVR (n = 8). Comparisons among different groups were done by means of ANOVA with Tukey's test. *$P < 0.05$; **$P < 0.01$; ***$P < 0.001$. Abbreviations as in Figure 1.

FIGURE 5 Myocyte Hypertrophy and Reversal After Pulmonary Valve Replacement

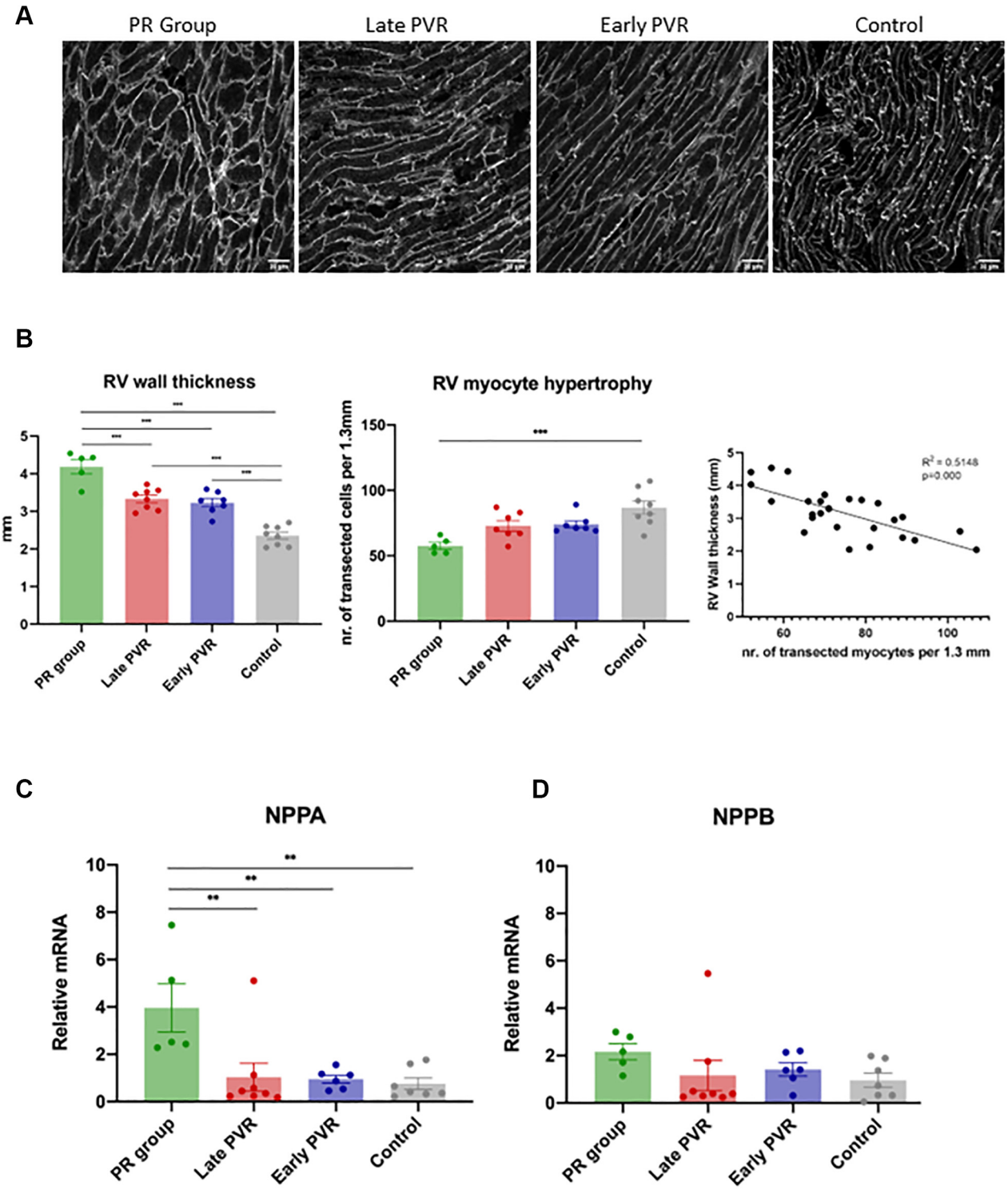

(A) Examples of 8-μm-thick sections for cardiac myocyte count. **(B)** Number of transected myocytes per 1.3 mm: PR (n = 5), late PVR (n = 7), early PVR (n = 7), control (n = 8). **(C)** NPPA and **(D)** NPPB expression in PR (n = 5), late PVR (n = 8), early PVR (n = 6), and control (n = 7) groups. Comparisons among different groups were done by means of ANOVA with Tukey's test. *$P < 0.05$; **$P < 0.01$; ***$P < 0.001$. Abbreviations as in Figures 1 and 2.

and fibrotic changes to the RV. PVR reverses these structural and fibrotic changes in the sheep rTOF model of PS and secondary PR. Although early valve replacement led to a quick RV recovery, eventually there was no difference in outcome between early and late valve replacement. These data support the benefit of valve replacement for RV function and suggest that there is a margin in the timing of the surgery.

ACKNOWLEDGMENTS The authors thank the KU Leuven TRANSfarm for their dedication to selecting, caring for, and providing the animals used for these experiments. They thank Medtronic for the Melody valves and Ensembles. We thank Numed for the CP-stents and BIB balloons.

FUNDING SUPPORT AND AUTHOR DISCLOSURES

This work was supported by the Foundation of Cardiac Surgery Research Belgium, an unrestricted grant from Medtronic, the Henri-Mertens Berx Foundation, and the National Fund for Scientific Research, Flanders. The authors have reported that they have no relationships relevant to the contents of this paper to disclose.

ADDRESS FOR CORRESPONDENCE: Dr Filip Rega, Department of Cardiac Surgery, University Hospitals Leuven, Herestraat 49, B-3000 Leuven, Belgium. E-mail: filip.rega@uzleuven.be.

PERSPECTIVES

COMPETENCY IN MEDICAL KNOWLEDGE: The long-term risks in patients with rTOF partially depend on chronic RV volume overload. Creation of a large-animal model resembling the course of patients with TOF enables unraveling the pathophysiologic observations of remodeling and reverse remodeling of the RV. Severe PR with RV volume load showed fibrotic changes and hypertrophy with increased signaling. PVR alters the fibrotic and hypertrophic changes with decreased gene expression promoting collagen cross-linking and remodeling of the ECM. Although early PVR led to a quick RV recovery, eventually there was no difference in outcome between early and late valve replacement.

TRANSLATIONAL OUTLOOK: In our sheep model, we could document, through tissue sampling, fibrosis related to PV regurgitation that correlated with PICP, which suggests further exploration of PICP in rTOF. The timing of valve implantation did not affect the eventual RV reverse remodeling process, calling for further clinical studies on optimal timing.

REFERENCES

1. Maury P, Sacher F, Rollin A, et al. Ventricular arrhythmias and sudden death in tetralogy of Fallot. *Arch Cardiovasc Dis*. 2017;110:354–362.

2. Cheung MMH, Konstantinov IE, Redington AN. Late complications of repair of tetralogy of Fallot and indications for pulmonary valve replacement. *Semin Thorac Cardiovasc Surg*. 2005;17:155–159.

3. Probst J, Diller G-P, Reinecke H, et al. Prevention of sudden cardiac death in patients with tetralogy of Fallot: risk assessment and long term outcome. *Int J Cardiol*. 2018;269:91–96.

4. Baumgartner H, de Backer J, Babu-Narayan SV, et al. 2020 ESC guidelines for the management of adult congenital heart disease. *Eur Heart J*. 2020;42:563–645.

5. Stout KK, Daniels CJ, Aboulhosn JA, et al. 2018 AHA/ACC guideline for the management of adults with congenital heart disease: a report of the American College of Cardiology/American Heart Association Task Force on Clinical Practice Guidelines. *J Am Coll Cardiol*. 2019;73(12):e81–e192.

6. Abbas JR, Hoschtitzky JA. Which is the best tissue valve used in the pulmonary position, late after previous repair of tetralogy of Fallot? *Interact Cardiovasc Thorac Surg*. 2013;17:854–860.

7. Bibevski S, Ruzmetov M, Fortuna RS, Turrentine MW, Brown JW, Ohye RG. Performance of SynerGraft decellularized pulmonary allografts compared with standard cryopreserved allografts: results from multiinstitutional data. *Ann Thorac Surg*. 2017;103:869–874.

8. Yong MS, Yim D, d'Udekem Y, et al. Medium-term outcomes of bovine jugular vein graft and homograft conduits in children. *Aust N Z J Surg*. 2015;85:381–385.

9. Cools B, Budts W, Heying R, et al. Medium term follow-up after percutaneous pulmonary valve replacement with the Melody valve. *IJC Heart Vasc*. 2015;7:92–97.

10. McElhinney DB, Hellenbrand WE, Zahn EM, et al. Short-and medium-term outcomes after transcatheter pulmonary valve placement in the expanded multicenter US melody valve trial. *Circulation*. 2010;122:507–516.

11. Dobbels B, Herregods MC, Troost E, et al. Early versus late pulmonary valve replacement in patients with transannular patch-repaired tetralogy of Fallot. *Interact Cardiovasc Thorac Surg*. 2017;25:427–433.

12. Alvarez-Fuente M, Garrido-Lestache E, Fernandez-Pineda L, et al. Timing of pulmonary valve replacement: how much can the right ventricle dilate before it loses its remodeling potential? *Pediatr Cardiol*. 2016;37:601–605.

13. Knauth AL, Gauvreau K, Powell AJ, et al. Ventricular size and function assessed by cardiac MRI predict major adverse clinical outcomes late after tetralogy of Fallot repair. *Heart*. 2008;94:211–216.

14. Therrien J, Provost Y, Merchant N, Williams W, Colman J, Webb G. Optimal timing for pulmonary valve replacement in adults after tetralogy of Fallot repair. *Am J Cardiol*. 2005;95:779–782.

15. Fuller S. Tetralogy of Fallot and pulmonary valve replacement: timing and techniques in the asymptomatic patient. *Semin Thorac Cardiovasc Surg Pediatr Card Surg Annu*. 2014;17:30–37.

16. Geva T. Indications for pulmonary valve replacement in repaired tetralogy of Fallot: the quest continues. *Circulation*. 2013;128:1855–1857.

17. Villafañe J, Feinstein JA, Jenkins KJ, et al. Hot topics in tetralogy of Fallot. *J Am Coll Cardiol*. 2013;62:2155–2166.

18. Heng EL, Gatzoulis MA, Uebing A, et al. Immediate and midterm cardiac remodeling after surgical pulmonary valve replacement in adults with repaired tetralogy of Fallot: a prospective cardiovascular magnetic resonance and clinical study. *Circulation*. 2017;136:1703–1713.

19. van der Ven JPG, van den Bosch E, Bogers AJCC, Helbing WA. Current outcomes and treatment of tetralogy of Fallot. *F1000Research*. 2019;8:1530. F1000 Faculty Rev.

20. Tretter JT, Friedberg MK, Wald RM, McElhinney DB. Defining and refining indications for transcatheter pulmonary valve replacement in patients with repaired tetralogy of Fallot: contributions from anatomical and functional imaging. *Int J Cardiol*. 2016;221:916–925.

21. Pagourelias ED, Daraban AM, Mada RO, et al. Right ventricular remodelling after transcatheter pulmonary valve implantation. *Catheter Cardiovasc Interv*. 2017;90:407–417.

22. Therrien J, Siu S, Harris L. Impact of pulmonary valve replacement on arrhythmia propensity late after repair of tetralogy of Fallot. *ACC Curr J Rev*. 2001;10:91.

23. Frangogiannis NG. Fibroblasts and the extracellular matrix in right ventricular disease. *Cardiovasc Res*. 2017;113:1453–1464.

24. Shinde AV, Humeres C, Frangogiannis NG. The role of α-smooth muscle actin in fibroblast-mediated matrix contraction and remodeling. *Biochim Biophys Acta Mol Basis Dis*. 2017;1863:298–309.

25. Alpat S, Yilmaz M, Onder S, et al. Histologic alterations in tetralogy of Fallot. *J Card Surg*. 2017;32:38–44.

26. Grothues F, Moon JC, Bellenger NG, Smith GS, Klein HU, Pennell DJ. Interstudy reproducibility of right ventricular volumes, function, and mass with cardiovascular magnetic resonance. *Am Heart J*. 2004;147:218–223.

27. Berman A. Effects of body surface area estimates on predicted energy requirements and heat stress. *J Dairy Sci*. 2003;86:3605–3610.

28. La Gerche A, Claessen G, Van De Bruaene A, et al. Cardiac MRI: a new gold standard for ventricular volume quantification during high-intensity exercise. *Circ Cardiovasc Imaging*. 2013;6:329–338.

29. Nagaraju CK, Dries E, Popovic N, et al. Global fibroblast activation throughout the left ventricle but localized fibrosis after myocardial infarction. *Sci Rep*. 2017;7:10801.

30. Nagaraju CK, Robinson EL, Abdesselem M, et al. Myofibroblast phenotype and reversibility of fibrosis in patients with end-stage heart failure. *J Am Coll Cardiol*. 2019;73:2267–2282.

31. Geens JH, Jacobs S, Claus P, et al. Partial mechanical circulatory support in an ovine model of post-infarction remodeling. *J Heart Lung Transplant*. 2013;32:815–822.

32. Bove T, Vandekerckhove K, Bouchez S, Wouters P, Somers P, van Nooten G. Role of myocardial hypertrophy on acute and chronic right ventricular performance in relation to chronic volume overload in a porcine model: relevance for the surgical management of tetralogy of Fallot. *J Thorac Cardiovasc Surg*. 2014;147:1956–1965.

33. Zeltser I, Gaynor JW, Petko M, et al. The roles of chronic pressure and volume overload states in induction of arrhythmias: an animal model of physiologic sequelae after repair of tetralogy of Fallot. *J Thorac Cardiovasc Surg*. 2005;130:1542–1548.

34. Lambert V, Capderou A, le Bret E, et al. Right ventricular failure secondary to chronic overload in congenital heart disease: an experimental model for therapeutic innovation. *J Thorac Cardiovasc Surg*. 2010;139:1197–1204.e1.

35. Agger P, Hyldebrandt JA, Nielsen EA, Hjortdal V, Smerup M. A novel porcine model for right ventricular dilatation by external suture plication of the pulmonary valve leaflets—practical and reproducible. *Interact Cardiovasc Thorac Surg*. 2010;10:962–966.

36. Robb JD, Harris MA, Minakawa M, et al. An ovine model of pulmonary insufficiency and right ventricular outflow tract dilatation. *J Heart Valve Dis*. 2012;21:247–252.

37. Yerebakan C, Klopsch C, Prietz S, et al. Pressure-volume loops: feasible for the evaluation of right ventricular function in an experimental model of acute pulmonary regurgitation? *Interact Cardiovasc Thorac Surg*. 2009;9:163–168.

38. Ko Y, Morita K, Abe T, Nakao M, Hashimoto K. Variability of pulmonary regurgitation in proportion to pulmonary vascular resistance in a porcine model of total resection of the pulmonary valve: implications for early- and long-term postoperative management of right ventricular outflow tract reconstruction with resulting pulmonary valve incompetence. *World J Pediatr Congenit Heart Surg*. 2015:6502–6510.

39. Gray R, Greve G, Chen R, et al. Right ventricular myocardial responses to chronic pulmonary regurgitation in lambs: disturbances of activation and conduction. *Pediatr Res*. 2003;54:529–535.

40. Kuehne T, Saeed M, Reddy G, et al. Sequential magnetic resonance monitoring of pulmonary flow with endovascular stents placed across the pulmonary valve in growing swine. *Circulation*. 2001;104:2363–2368.

41. Ersboell M, Vejlstrup N, Nilsson JC, et al. Percutaneous pulmonary valve replacement after different duration of free pulmonary regurgitation in a porcine model: effects on the right ventricle. *Int J Cardiol*. 2013;167:2944–2951.

42. Kjaergaard J, Iversen KK, Vejlstrup NG, et al. Effects of chronic severe pulmonary regurgitation and percutaneous valve repair on right ventricular geometry and contractility assessed by tissue Doppler echocardiography. *Echocardiography*. 2010;27:854–863.

43. Wang T, Ma J, Hogan AN, et al. Quantitative translation of dog-to-human aging by conserved remodeling of epigenetic networks. *bioRxiv*. Posted online November 4, 2019. https://doi.org/10.1101/829192.

44. Verbelen T, Claus P, Burkhoff D, et al. Low-flow support of the chronic pressure-overloaded right ventricle induces reversed remodeling. *J Heart Lung Transplant*. 2018;37:151–160.

45. Kim W, Kwak JG, Kwon HW, et al. Pulmonary valve replacement may not restore ventricular volume and functional status in patients with pulmonary regurgitation after late tetralogy of Fallot repair. *Eur J Cardiothoracic Surg*. 2021;61:64–72.

46. Morris RA, Damon B, Mironov V, et al. Periostin regulates collagen fibrillogenesis and the biomechanical properties of connective tissues. *J Cell Biochem*. 2007;101:695–711.

47. Snider P, Standley KN, Wang J, Azhar M, Doetschman T, Conway SJ. Origin of cardiac fibroblasts and the role of periostin. *Circ Res*. 2009;105:934–947.

48. Chen CA, Tseng WYI, Wang JK, et al. Circulating biomarkers of collagen type I metabolism mark the right ventricular fibrosis and adverse markers of clinical outcome in adults with repaired tetralogy of Fallot. *Int J Cardiol*. 2013;167,2963-298.

49. Chen CA, Dusenbery SM, Valente AM, Powell AJ, Geva T. Myocardial ECV fraction assessed by CMR is associated with type of hemodynamic load and arrhythmia in repaired tetralogy of Fallot. *J Am Coll Cardiol Img*. 2016;9:1–10.

50. Yamamura K, Yuen D, Hickey EJ, et al. Right ventricular fibrosis is associated with cardiac remodelling after pulmonary valve replacement. *Heart*. 2019;105:855–863.

51. Kozak MF, Redington A, Yoo SJ, Seed M, Greiser A, Grosse-Wortmann L. Diffuse myocardial fibrosis following tetralogy of Fallot repair: a T1 mapping cardiac magnetic resonance study. *Pediatr Radiol*. 2014;44:403–409.

52. Babu-Narayan SV, Kilner PJ, Li W, et al. Ventricular fibrosis suggested by cardiovascular magnetic resonance in adults with repaired tetralogy of Fallot and its relationship to adverse markers of clinical outcome. *Circulation*. 2006;113:405–413.

KEY WORDS fibrosis, repaired tetralogy of Fallot, ovine, reverse remodeling, right ventricle

APPENDIX For supplemental tables, please see the online version of this paper.